Supplemental Information for "Kinetic Modelling of Voltage Dependent Gating in Funny Channels"

Delbert Yip[1] and Eric Accili[1]

[1] *Department of Cellular and Physiological Sciences, University of British Columbia, Vancouver, British Columbia V6T 1Z3, Canada.*

These supplemental notes provide details for modelling results shown in Figure 2 of the main text. The relevant files and generating code can be found at: https://github.com/haganenoneko/FunnyChannelGatingReview.

Contents

1 Model Parameterization

As described in the main text, the mutant and wild-type data were fit using four- and six-state models. The formulations of each model were derived from Chen et al. (2007) and Hummert et al. (2018), respectively. For the mutant data, the six-state model did not improve the fit using the four-state model, so only the best-fit parameters for latter have been reported (Figure 1). For the wild-type data, the six-state model fit better than the four-state model, and best-fit parameters for both models are reported in Figure 1.

The full expression of voltage-dependent rates in the six-state ("Hummert") model is identical to those given for the four-state ("Chen") model (Figure

1A). However, the 'slope' factors were constrained to reduce the number of free parameters. That is,

$$k(V) = k^0 \exp(\pm V/s)$$

is a generic voltage-dependent rate with coefficient k_0 and slope s. In the Hummert model, s was identical for all rates with the same subscript ($_a$ or $_b$). For instance, s was identical for transitions $C_1 \leftrightarrow C_2$ and $O_1 \leftrightarrow O_2$.

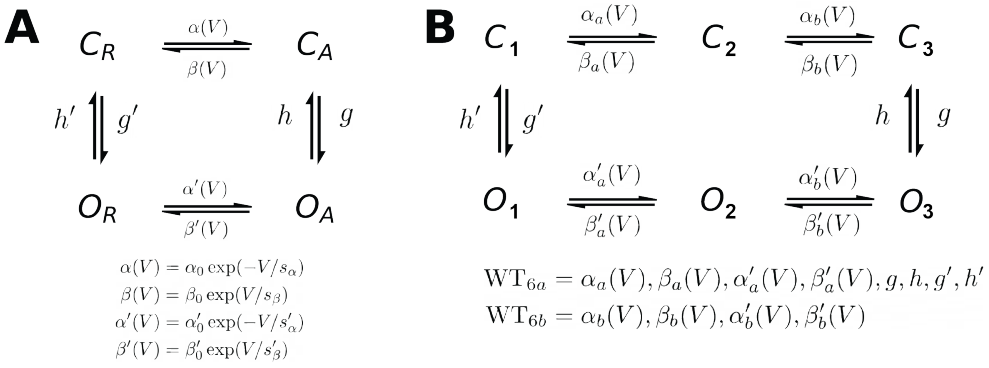

C

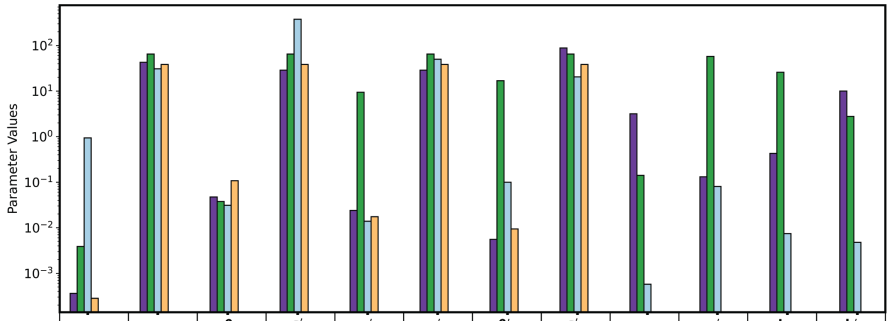

	α_0	s_α	β_0	s'_β	α'_0	s'_α	β'_0	s'_β	g	g′	h	h′
WT_6b	2.8e-04	3.8e+01	1.1e-01	3.8e+01	1.7e-02	3.8e+01	9.4e-03	3.8e+01	nan	nan	nan	nan
WT_6a	3.9e-03	6.5e+01	3.8e-02	6.5e+01	9.4e+00	6.5e+01	1.7e+01	6.5e+01	1.4e-01	5.8e+01	2.6e+01	2.8e+00
Mutant	9.4e-01	3.1e+01	3.1e-02	3.8e+02	1.4e-02	5.0e+01	1.0e-01	2.0e+01	5.7e-04	8.0e-02	7.4e-03	4.8e-03
WT_4	3.6e-04	4.3e+01	4.7e-02	2.9e+01	2.4e-02	2.9e+01	5.6e-03	8.8e+01	3.2e+00	1.3e-01	4.3e-01	1.0e+01

Figure 1: **Models and best-fit parameter values.**
(A) Schematic for the four-state model, as per Chen et al. (2007).
(B) Schematic of the six-state model, as in Hummert et al. (2018). Note that the parameterization used here differs from that used by Hummert et al. (2018). See the supplementary text for details.
(C) Best-fit parameter values for fitting of mutant data with the four-state model ("Mutant"), wild-type data with the four-state model ("WT_4"), and wild-type data with the six-state model ("WT_6a" and "WT_6b"). To enable comparison between the four- and six-state model parameters, the six-state parameters have been split into two parameter sets, which are defined in (B).

1.1 Detailed Balance

The use of identical slope values in the Hummert model allows the model to satisfy detailed balance at all non-zero voltages. Detailed balance at 0 mV can then be established by choosing any of the voltage-dependent 'coefficient' terms, or one of the voltage-independent parameters.

Chen et al. (2007) did not constrain their slopes, but instead used s'_α and α'_0 to establish detailed balance. Hummert et al. (2018) used constrained slopes and h of the $O_1 \rightarrow C_1$ transition to set detailed balance. Here, we set detailed balance in the four-state model using s'_α and α'_0, and g' in the six-state model.

2 Model Optimization

2.1 Data Preparation

The experimental data used for modelling was digitized from Figures 4A and 4B from Ramentol et al. (2020) using WebPlotDigitizer. The data were digitized to an approximate frequency of 2 kHz. However, not all traces could be digitized. For instance, deactivating tail currents were often not digitized because they overlapped for multiple test voltages.

After digitization, the data were normalized using computed G-V and F-V data, which were provided in the Supplementary Information of the original publication (Ramentol et al, 2020). The lowest and highest values of opening and activation from the G-V and F-V data, respectively, were then used to normalize the digitized time courses. A similar procedure was previously described in Chen et al. (2007).

2.2 Modelling Methods

A variety of models were implemented by specifying their transition matrices and related information in separate scripts, and then called using a main script containing simulation/optimization methods. Model calibration (parameter fitting) was done entirely using scripts written in Julia 1.4.0.

All kinetic models used follow the chemical 'master' equation: $\frac{d\mathbf{x}}{dt} = \mathbf{A}\mathbf{x}$, where $\mathbf{x}$ is a vector of states and $\mathbf{A}$ denotes the transition matrix. The elements of $\mathbf{A}$ are defined as:

$A_{ij} = k_{ji}$ for $i \neq j$, where k_{ji} is the rate from state j to state i.

$A_{ii} = -\sum_{\substack{j=1 \\ i \neq j}}^{N} k_{ij}$ for $i = j$, where N is the total number of states.

We also have that $\sum_{i=1}^{N} x_i = 1$, so the number of equations can be reduced by one, yielding a modified form of the 'master' equation:

$$\frac{d\mathbf{x}}{dt} = \mathbf{A}_{N-1}\ \mathbf{x}_{N-1} + \mathbf{k} \tag{1}$$

where the subscript $N-1$ indicates that the reduced dimensionality of the respective quantities. $\mathbf{k}$ is a vector containing rates from the state which was removed.

The steady-state distribution $\mathbf{x}_\infty$ can be obtained by, for instance, computing the eigenvector of $\mathbf{A}$ that has eigenvalue zero, and then dividing by its sum. For the $(N-1)$-dimensional system above, we have:

$$\mathbf{x}_\infty = -\mathbf{A}_{N-1}^{-1}\mathbf{k} \tag{2}$$

Finally, depending on the type of data (current or fluorescence), we multiply the trajectories of $x(t)$ by appropriate 'observation' vectors, which acts to sum the states of interest: open states for current traces and activated states for fluorescence traces.

2.3 Numerical methods

Simulations were initialized from the steady-state using the methods above, at respective holding potentials, and then solved by numerical integration using a stiff solver (TR-BDF2). Absolute and relative tolerances were set to 1e-8 to avoid settling into local optima (Clerx et al., 2019).

2.4 Optimization

Model calibration was done by minimizing a squared error cost function using the implementation of Covariance Matrix Adaptive Evolution Strategy (CMAES) in GCMAES.jl, with gradients computed by autodifferentiation using ForwardDiff.jl.

The mean of the sum of squared errors (MSE) was used as the cost function in optimization. Separate MSEs were computed for the current and fluorescence, with the total cost given by:

$$\mathrm{MSE}_{\mathrm{total}} = p_I\ \mathrm{MSE}_I + p_F\ \mathrm{MSE}_F \tag{3}$$

Where, the subscripts I and F refer to current and fluorescence data, respsectively. The coefficients p_I and p_F are proportions that sum to one and were sometimes used to to alter the weight assigned to current versus fluorescence data. For instance, due to limitations in data digitization, the wild-type data contained more time courses for fluorescence than for current. Thus, proportions p_D were used to place more weight on the current data and lower that

on the fluorescence data. The MSE for a given trace of current or fluorescence data was computed using:

$$\text{MSE} = \frac{\sum_{i=1}^{N}(x_i - \hat{x})^2}{N} \tag{4}$$

Where, x and $\hat{x}$ denote the data and model output, respectively, and N is the total number of data points.

3 References

Chen, S., Wang, J., Zhou, L., George, M.S., Siegelbaum, S.A., 2007. Voltage sensor movement and cAMP binding allosterically regulate an inherently voltage-independent closed-open transition in HCN channels. J. Gen. Physiol. 129, 175–188. https://doi.org/10.1085/jgp.200609585

Clerx, M., Beattie, K.A., Gavaghan, D.J., Mirams, G.R., 2019. Four Ways to Fit an Ion Channel Model. Biophysical Journal 117, 2420–2437. https://doi.org/10.1016/j.bpj.2019.08.001

Hummert, S., Thon, S., Eick, T., Schmauder, R., Schulz, E., Benndorf, K., 2018. Activation gating in HCN2 channels. PLoS Comput. Biol. 14, e1006045. https://doi.org/10.1371/journal.pcbi.1006045

Ramentol, R., Perez, M.E., Larsson, H.P., 2020. Gating mechanism of hyperpolarization-activated HCN pacemaker channels. Nat Commun 11, 1419. https://doi.org/10.1038/s41467-020-15233-9